Research Article

A MIMO-OFDM Testbed, Channel Measurements, and System Considerations for Outdoor-Indoor WiMAX

Víctor P. Gil Jiménez,[1] M. Julia Fernández-Getino García,[1] Ana García Armada,[1] Rafael P. Torres,[2] Juan José García Fernández,[1] Matilde P. Sánchez-Fernández,[1] Marta Domingo,[2] and Oscar Fernández[2]

[1] *Signal Theory and Communications Department, Universidad Carlos III de Madrid, Avenida de la Universidad 30, 28911, Madrid, Spain*

[2] *Communications Engineering Department, Universidad de Cantabria, Avenida de los Castros s/n., 39005 Santander, Spain*

Correspondence should be addressed to Víctor P. Gil Jiménez, vgil@tsc.uc3m.es

The design, implementation, and test of a real-time flexible 2×2 (Multiple Input Multiple Output-Orthogonal Frequency Division Multiplexing) MIMO-OFDM IEEE 802.16 prototype are presented. For the design, a channel measurement campaign on the 3.5 GHz band has been carried out, focusing on outdoor-indoor scenarios. The analysis of measured channels showed that higher capacity can be achieved in case of obstructed scenarios and that (Channel Distribution Information at the Transmitter) CDIT capacity is close to (Channel State Information at the Transmitter) CSIT with much lower complexity and requirements in terms of channel estimation and feedback. The baseband prototype used an (Field Programmable Gate Array) FPGA where enhanced signal processing algorithms are implemented in order to improve system performance. We have shown that for MIMO-OFDM systems, extra signal processing such as enhanced joint channel and frequency offset estimation is needed to obtain a good performance and approach in practice the theoretical capacity improvements.

1. Introduction

The potential of MIMO (Multiple Input Multiple Output) systems combined with OFDM (Orthogonal Frequency Division Multiplexing) in terms of spectral efficiency has configured this technology as a perfect candidate for many wireless systems in development [1, 2]. Specifically, the extension of the traditional local area network systems to metropolitan coverage networks (WMAN, Wireless Metropolitan Area Network) considers the deployment of multiple antennas, and in these scenarios, novel channel environments such as the combination of outdoor-indoor come up. The reference standard family for metropolitan area networks is the IEEE 802.16 [3] where IEEE 802.16-2004 [4] and IEEE 802.16e address broadband wireless access systems with a MIMO-OFDM physical layer [5].

One of the issues that should be taken into account when deploying multiple antennas is, in general, to choose the best transmission strategy (which makes for the best use in terms of spectral efficiency) for the degrees of freedom provided by spatial diversity. This transmission strategy will clearly depend on which information we have available at the transmitter and also on the channel scenarios that eventually make the transmission modes available.

In order to be able to characterize and optimize the system performance in realistic conditions, we have developed a testbed and carried out a channel measurement campaign. The testbed includes the main features of the IEEE 802.16 standard, also with the aim of further developing (in terms of performance) and contemplating other strategies that are not explicitly available in the specification, such as different channel knowledge scenarios at the transmitter, and the comparison between two transmission strategies such as beamforming (BF) and spatial multiplexing (SM).

Several testbeds for MIMO [6–11] and MIMO-OFDM [12–16] have been reported in literature. In [6–8] three
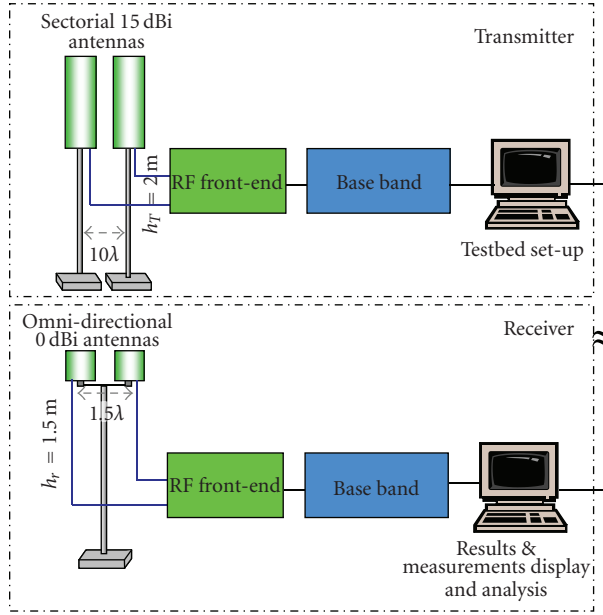
(a) General Block diagram of the testbed
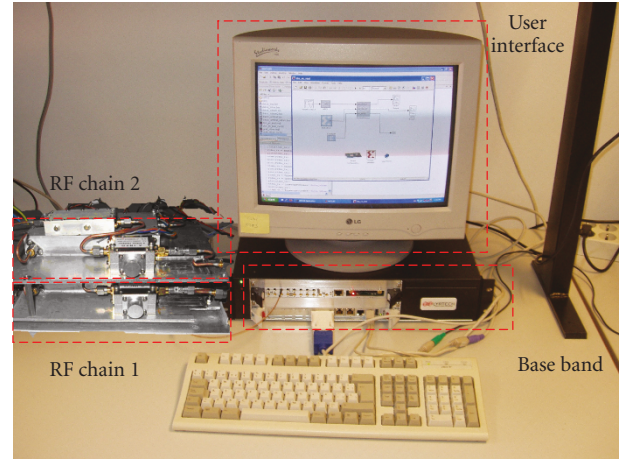
(b) Transmitter testbed picture

Figure 1: Testbed.

MIMO testbeds are implemented for the evaluation of realistic improvements in performance of theoretical MIMO results [10]. The first one used FPGA (Field Programmable Gate Array), whereas the second one used a DSP (Digital Signal Processor), showing that both architectures are good enough to implement a real MIMO system. Indeed, in [8, 9] from the same authors, a joint architecture is used to leverage on both capabilities, and it is applied to HSDPA (High Speed Data Packet Access). Further, in [11], a comparison of different architectures for MIMO testbeds based on FPGA, DSP, ASIC (Application-Specific Integrate-Circuit), or mixed DSP + FPGA is presented. Extending to MIMO-OFDM, in [12], a generic platform is implemented to show the realistic improvements for 2×3 and 1×3 schemes with SM, STC (Space Time Coding), MRC (Maximum Ratio Combining), and Adaptive Modulation (AM). In [14, 16], two extensions to the IEEE 802.11a standard [17] for multiple-antenna testbeds are presented, the first one with the base-band processing off-line in a computer, and the second one with all the base-band processing in the FPGA. Finally, in [13, 15], IEEE 802.16-like-based MIMO-OFDM platforms are presented. The first case focuses on the transmission schemes such as Hybrid ARQ (Automatic Repeat reQuest) and the second case on the BLAST (Bell Labs lAyered Space Time) architectures. In this paper, we describe a 2×2 flexible IEEE 802.16-based platform that is implemented for the evaluation of the transmission schemes in the standard, the algorithms for channel estimation and synchronization, and, moreover, designing and testing new schemes and algorithms for a MIMO-OFDM system.

As discussed in [12], STBCs (Space Time Block Codes) are attractive since they require no feedback and allow linear decoding at the receiver. We have selected an Alamouti

scheme [18] for the basic testbed, since it is suitable for a 2×2 configuration and it was the first choice in the standard [4]. Extensions to other STBC such as [19] are straightforward since the algorithms developed for channel estimation and synchronization can work with any number of antennas provided that the transmitted streams are orthogonal. Only the pilot pattern should be slightly modified.

Besides, an extensive channel measurements campaign has been carried out and considerations about the system for the outdoor-indoor scenario have been documented.

The rest of the paper is structured as follows. In Section 2, the general features of the testbed are presented and the main design decisions concerning RF and Baseband modules are discussed. In Section 3, the outdoor-indoor measurement system, scenarios, and capacity obtained for WMAN are given. In Section 4, some performance results are analyzed and finally some conclusions are outlined in Section 5.

Note. Throughout the paper the following notation will be used. Bold capitals and bold will be used for matrices and vectors, respectively. $E\{\cdot\}.*,^T,^H$, and $\mathrm{Tr}\{\cdot\}$ are the expectation, the conjugate, the transpose, the Hermitian, and the trace operators, respectively, and $\mathrm{diag}\{\mathbf{x}\}$ is a diagonal matrix with the elements in its diagonal equal to $\mathbf{x}$ and 0 elsewhere.

2. Description of the Testbed

In this paper, we present a 2×2 MIMO-OFDM transmission/reception scheme that has been implemented and tested. A high-level block diagram is depicted in Figure 1(a). A binary stream can be generated either by the user from the computer or randomly by the system. Data are passed first by the BB (Base-Band) block which processes on-line all the BB

and up-converts to 70 MHz of IF (Intermediate Frequency). After that, signals are fed to the RF (Radio Frequency) block to be transmitted at 3.5 GHz. At the receiver, the same counterpart blocks have been implemented. Since the transmitter and the receiver can be physically separated, both are connected to a LAN (Local Area Network) by the computers that act as user interface and data storage. Also in this section, a system design is presented to summarize some of the common system parameters and provide a brief description of the IEEE 802.16 standard. A picture of the transmitter prototype is shown in Figure 1(b).

2.1. System Design.

The MIMO-OFDM system presented in the following section is based on the OFDM physical layer defined in the IEEE 802.16 standard [4] and the MIMO extension in [5]. The standard defines several bandwidths, but in this testbed, the 3.5 MHz configuration has been chosen. The number of subcarriers (N) for the OFDM layer is $N = 256$ and a CP (Cyclic Prefix) length of $N_{CP} = 64$ samples is considered. Although the scheme has been designed to be flexible and for further extensions to $n_T \times n_R$ antennas, where n_T and n_R are the number of transmit and receive antennas, respectively, in this testbed n_T and n_R have been both fixed to two, that is, $n_T = n_R = 2$.

2.1.1. Frame Structure.

The system is frame based and the number of OFDM symbols transmitted per frame can be defined by the user. The standard proposes seven transmission modes combining modulations from BPSK, QPSK, 16QAM, and 64QAM with different code rates $R_c = 1/2, 2/3,$ and $3/4$. For this testbed, the frame has been configured to have 10 OFDM symbols per frame.

The IEEE 802.16 standard provides two different preambles, the *long preamble* (two identical OFDM symbols) and the *short preamble* (one OFDM symbol). When diversity is used, only the *short preamble* can be used. This preamble is based on a fixed sequence of a 128-sample length that is BPSK modulated and transmitted on even subcarriers on antenna 1 and odd subcarriers on antenna 2. Thus, they are orthogonal in frequency and the time structure is a 256-sample length sequence with two identical halves. This preamble will be used for timing synchronization, frequency offset, and channel estimation. Prior to the channel and frequency offset estimation, a time synchronization is needed. Since the time-domain IEEE 802.16 preamble is an OFDM symbol with two equal halves, algorithms based on metrics such as [20], based on [21, 22], are applied.

Next, we explain the channel and frequency offset algorithm that have been tailored to the WiMAX signal structure.

2.1.2. Channel and Frequency Offset Estimation.

One of the most important problems in MIMO channel estimation is that we have to estimate the $n_T \times n_R$ SISO (Single Input Single Output) channels and the effect from the other channels must be previously removed. Several methods and algorithms have been proposed to perform channel estimation. In this testbed, the LS (Least Squares) method

in [23] adapted to MIMO as in [24] has been used. This algorithm is data aided based on the available IEEE 802.16 preamble in the transmission. The main objective is to estimate the L channel taps for the $n_T \times n_R$ channels (based on the channel measurements campaign, we assume that we know the number of taps), that is, the estimation of $n_T \times n_R \times L$ coefficients. Since there is only one OFDM symbol preamble when diversity is used in the IEEE 802.16 standard, the following constraint must be fulfilled:

$$N_p \geq n_T \times L, \tag{1}$$

where N_p is the number of pilot subcarriers in the preamble and L is the channel length. In order to avoid ISI (Inter Symbol Interference), $N_{CP} > L$. In the standard, the number of pilot subcarriers is 128, that is, $N_p = 128$, and therefore channels up to $L = 64$ (very rich scattering channels) can be accurately estimated.

After the signal is time synchronized, the frequency-domain received signal preamble at ith antenna ($i = 1 \cdots n_R$) can be expressed as

$$\mathbf{y_i} = \sum_{j=1}^{n_T} \mathbf{P_j} \mathbf{F} \check{\mathbf{h}}_{i,j} + \mathbf{w_i}, \tag{2}$$

where $\mathbf{y_i} \in \mathbb{C}^{N \times 1}$, $\mathbf{P_j} \in \mathbb{C}^{N \times N} = \text{diag}\{\mathbf{p_j}\}$, $j = 1 \cdots n_T$, $\mathbf{p_j} \in \mathbb{C}^{N \times 1}$ is the frequency-domain preamble for the transmit antenna j, $\mathbf{F} \in \mathbb{C}^{N \times N} = (1/N)(e^{-j2\pi kn/N})_{k,n=0,0}^{N-1,N-1}$ is the DFT operation matrix, $\check{\mathbf{h}}_{i,j}$ is the zero-padded time-domain channel taps $\mathbf{h}_{i,j} \in \mathbb{C}^{L \times 1}$ from jth transmit antenna to receive antenna i, that is, $\check{\mathbf{h}}_{i,j} \in \mathbb{C}^{N \times 1} = [\mathbf{h}_{i,j}^T \mathbf{0}_{(N-L \times 1)}^T]^T$, and $\mathbf{w_i} \in \mathbb{C}^{N \times 1}$ is the frequency-domain Additive White Gaussian Noise (AWGN) samples for each subcarrier with variance σ^2. Defining the time-domain channel response for ith receive antenna $\mathbf{h_i} \in \mathbb{C}^{n_T \cdot L \times 1}$ including all the SISO channels for one receive antenna i as $\mathbf{h_i} = [\mathbf{h}_{i,1}^H, \mathbf{h}_{i,2}^H, \ldots, \mathbf{h}_{i,n_T}^H]^H$ and a matrix $\mathbf{A} \in \mathbb{C}^{N \times n_T \cdot L}$ as $\mathbf{A} = [\mathbf{FP_1}, \mathbf{FP_2}, \ldots, \mathbf{FP_{n_T}}]$, the received signal at ith antenna can be rewritten as

$$\mathbf{y_i} = \mathbf{A}\mathbf{h_i} + \mathbf{w_i}. \tag{3}$$

Each SISO time-domain channel estimation $\hat{\mathbf{h}}_\mathbf{i} \in \mathbb{C}^{n_T \cdot L \times 1}$ can be obtained by applying the LS method as

$$\hat{\mathbf{h}}_\mathbf{i} = \mathbf{A}^+ \mathbf{y_i}, \tag{4}$$

and $\mathbf{A}^+ \in \mathbb{C}^{n_T \cdot L \times N}$ is the pseudoinverse of $\mathbf{A}$ defined as

$$\mathbf{A}^+ = (\mathbf{A}^H \mathbf{A})^{-1} \mathbf{A}^H, \tag{5}$$

which can be precalculated and stored on the receiver side. It should be noted that this is only possible if matrix $\mathbf{A}$ is full rank, and this is why (1) must be fulfilled. Since only half of the samples (even or odd) in the frequency-domain IEEE 802.16 preamble are pilots, zero-samples must be removed from the operations, and according to [24], the time-domain LS estimation is obtained as

$$\hat{\mathbf{h}}_{LS,i} = (\tilde{\mathbf{F}}^H \tilde{\mathbf{P}}^H \tilde{\mathbf{P}} \tilde{\mathbf{F}})^{-1} \tilde{\mathbf{F}}^H \tilde{\mathbf{P}}^H \mathbf{F}_n \tilde{\mathbf{y}}_i, \tag{6}$$
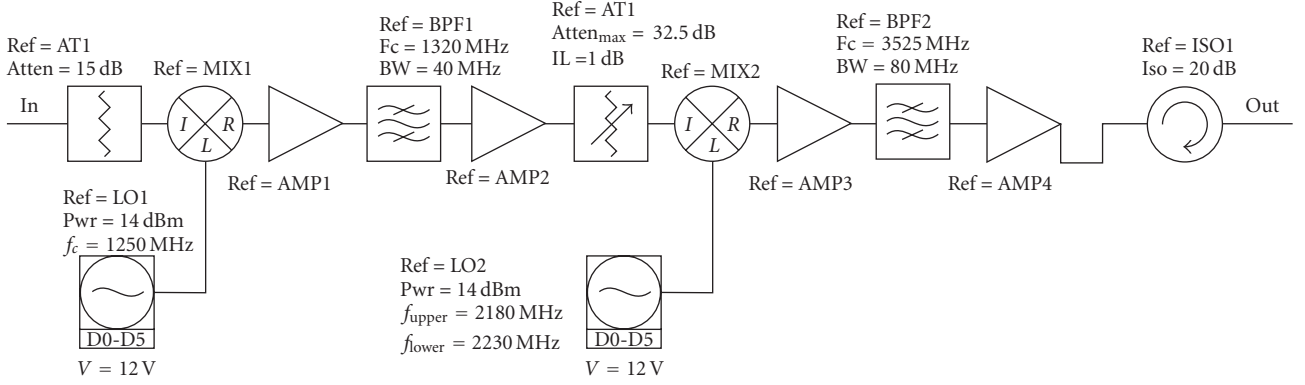
FIGURE 2: Radio Frequency TX Chain Modules Diagram.

where $\widetilde{\mathbf{F}} \in \mathbb{C}^{N/2 \times N_{\mathrm{CP}}}$ are the first N_{CP} columns from $\mathbf{F}_n$, $\mathbf{F}_n \in \mathbb{C}^{N/2 \times N/2}$ is the DFT matrix $\mathbf{F}$ removing the rows whose index corresponds to a zero element in the preamble, $\widetilde{\mathbf{P}} \in \mathbb{C}^{N/2 \times N/2} = \mathrm{diag}\{\mathbf{p}_n\}$, with $\mathbf{p}_n$ the vector of nonzero elements in $\mathbf{p}_j$, and $\widetilde{\mathbf{y}}_i \in \mathbb{C}^{N/2 \times 1}$ is the time-domain preamble received by ith antenna. Next, the most L significant taps are kept (i.e., the first L values), this way avoiding noise caused by nonexistent taps.

This estimator is unbiased and its Mean Square Error (MSE) can be calculated as

$$\mathrm{MSE}_i = \frac{\sigma^2}{n_{\mathrm{T}} L} \mathrm{Tr}\left\{ \left[(\mathbf{A}^+)^H (\mathbf{A}^+)^H \mathbf{A}^+ \right]^{-1} \right\}. \tag{7}$$

The channel equalization is performed in the frequency-domain using the Zero-Forcing technique as follows:

$$\hat{\mathbf{y}}_i|_{\mathrm{ZF}} = \left[\left(\hat{\mathbf{h}}_{\mathrm{LS},i}^N \right)^H \hat{\mathbf{h}}_{\mathrm{LS},i}^N \right]^{-1} \hat{\mathbf{h}}_{\mathrm{LS},i}^N \mathbf{y}_i. \tag{8}$$

In order to obtain the frequency channel response $\hat{\mathbf{h}}_{i,j}^N \in \mathbb{C}^{N \times 1}$, a DFT operation over the zero-padded time frequency response $\check{\mathbf{h}}_{i,j}^N = [\hat{\mathbf{h}}_{i,j}^T \ \mathbf{0}_{(N-L \times 1)}^T]^T$ is performed:

$$\hat{\mathbf{h}}_{i,j}^N = \mathbf{F} \check{\mathbf{h}}_{i,j}^N. \tag{9}$$

Since the channel estimation is executed at the beginning of the packet and used during the whole packet transmission, these operations are only performed once. This way, part of the frequency offset will be estimated and compensated by the channel estimation and equalization. To increase performance, a residual normalized (to the frequency spacing (Δf), that is, $\varepsilon = f_\varepsilon(\mathrm{Hz}) / \Delta f(\mathrm{Hz})$) frequency offset estimation is performed:

$$\hat{\varepsilon} = \sum_{n=0}^{127} \left[\widetilde{y}_{i,1}[n] \cdot \widetilde{y}_{i,1}'[n]^* \right]^* \cdot \left[\widetilde{y}_{i,2}[n] \cdot \widetilde{y}_{i,2}'[n]^* \right], \tag{10}$$

where n is the time index, $\widetilde{y}_{i,j}$ is the time-domain received signal from jth transmit antenna at ith receive antenna, the upper limit of the summation is due to the fact that the IEEE 802.16 standard uses $N = 256$ sub-carriers, and thus, if sampling at one sample per symbol, the second part of the

preamble will start at 128th sample and $\widetilde{y}_{i,j}'$ is the ideal time-domain received signal if the channel estimation was perfect:

$$\widetilde{y}_{i,1}'[n] = \sum_{j=1}^{n_{\mathrm{T}}} \sum_{\ell=0}^{L-1} h_{i,j}[\ell] \cdot q_j[n-k],$$

$$\widetilde{y}_{i,2}'[n] = \sum_{j=1}^{n_{\mathrm{T}}} \sum_{\ell=0}^{L-1} h_{i,j}[\ell] \cdot q_j[n+128-k], \tag{11}$$

where $q_j[n]$ is the nth time-domain transmitted pilot by antenna j.

After the correction of the estimated frequency offset, the channel estimation is performed again to enhance the system performance. This new estimation will be referred to throughout the paper as enhanced estimation.

2.1.3. Subsampling. Usually, signals are sampled at least two times the Nyquist sampling frequency (i.e., $f_s \geq 2W_T$, where W_T is the total signal bandwidth $W_T = f_c + W$, where f_c is the carrier frequency, and W is the signal bandwidth). However, sometimes such a large f_s is not possible, and, thus, subsampling needs to be applied [25]. If the signal has a bandwidth of W Hertz, sampling at $f_s' \geq 2W$ is enough to recover the original signal without distortion (aliasing).

2.2. Radio Frequency Module. The RF module provides two identical chains (one per antenna) both for transmitter and receiver. However, the amplitude imbalance between both is very low (<0.23 dB for the transmitter and <0.8 dB for the receiver), whereas the phase imbalance is 0. We must note the demanding requirements on VSWR (Voltage Standing Wave Ratio), especially at the transmitter, which required the use of an isolator of 20 dB. Also, the gain ripple is important because signals are OFDM based. In what follows, the transmit and receive chain will be described in more detail. A summary of the specifications can be found in Table 1.

2.2.1. Transmitter. A block diagram for one out of two of the transmit chains is shown in Figure 2. It should be noted

TABLE 1: RF specifications Summary.

Description	Receiver	Transmitter
Noise Figure	<8.5 dB	—
Linear Gain	78 dB	14.4 dB
Gain Ripple	<0.9 dBpp	<1 dBpp
Output Power	20 dBm	30 dBm
Spurious	< -52 dBc @ $P_{out} = 0$ dBm, $G = 71$ dB	< -74 dBc
Phase Noise	< -84 dBc/Hz @1 kHz	< -90 dBc/Hz @1 kHz
	< -88.5 dBc/Hz @10 kHz	< -91 dBc/Hz @10 kHz
	< -107 dBc/Hz @100 kHz	< -115 dBc/Hz @100 kHz
Output VSWR	< -18.5 dB	<17.5 dB
Input VSWR	< -15.5 dB	-30 dB
Amplitude Imbalance between chains	<0.8 dB	<0.23 dB
Phase Imbalance between chains	0.0	0.0
Frequency Stability	—	2.5 ppm
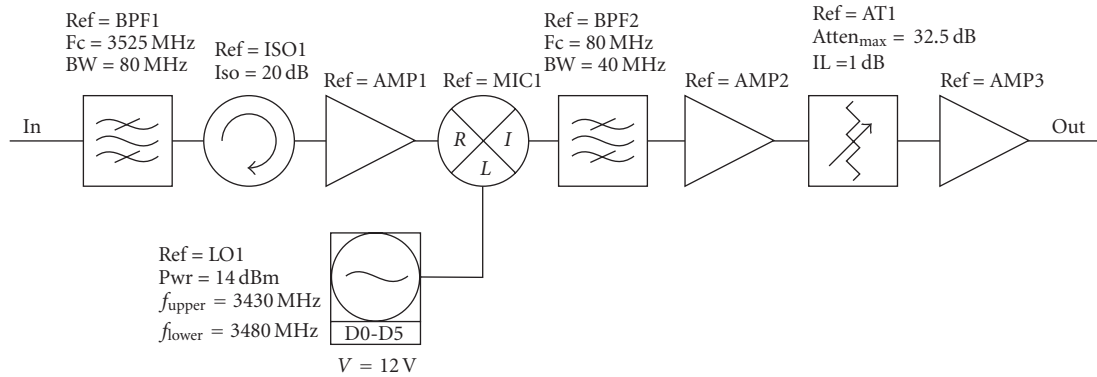
FIGURE 3: Radio Frequency Chain RX Modules Diagram.

that both chains share local oscillators. As mentioned before, the signal from IF is 70 MHz. In order to interface with the base-band module and to adapt gains, first an attenuator is placed. Afterwards, two up-conversions are performed, one at 1.25 GHz and the second one on the 3.5 GHz band. A variable gain is placed in between both to be able to control the chain gain. Next, a band-pass filter is applied to transmit only the signal of interest and to avoid the transmission of spurious. An isolator is used just in front of the antenna to avoid the reception of other signals (such as the one transmitted by the other antenna).

2.2.2. Receiver. A block diagram for one out of two of the receive chains is shown in Figure 3. Again, both chains share the local oscillator. A band-pass filter is placed behind the antenna in order to avoid image frequency and the reception of other uncontrollable signals that might cause the saturation of the amplifiers. Another isolator is used to avoid the reflections of the up-conversion process. As such, there is only one up-conversion to the target frequency of 3.5 GHz. Another band-pass filter is applied to suppress the different generated signals from the mixer, and then, in order to act as interface with the base-band module and to be able to control the gain, an attenuator is used.

2.3. Base-Band and Intermediate Frequency Modules. Next, the Base-Band and Intermediate Frequency modules will be described. Both modules have been implemented using similar hardware, the DAC-VHS and the ADC-VHS from Lyrtech for the transmitter and receiver, respectively. Both platforms are analogous in hardware with the difference that the first one has 8 DACs (Digital to Analog Converters) with 14-bit precision while the second one has 8 ADCs (Analog to Digital Converters) with 14-bit precision. For the testbed, only 2 out of 8 are used but the platform allows extensions for more than 2 antennas. Each board has a large Virtex IV FPGA from Xilinx and a Pentium IV processor. The FPGA was used for the prototype implementation and base-band processing whereas the processor was used for managing and user interface purposes.

Since the Radio Frequency module required 70 MHz inputs, the interface between the BB and the RF part has the mission not only of adapting impedances and voltages but also of up/down-converting the BB to/from 70 MHz of intermediate frequency. Another technical aspect in the receiver was that the maximum ADC sample frequency (104 Msamples/s) was not enough to fulfill the Nyquist criterion for the 70 MHz signal; thus, a subsampling processing was needed to be able to correctly receive the signal. In our
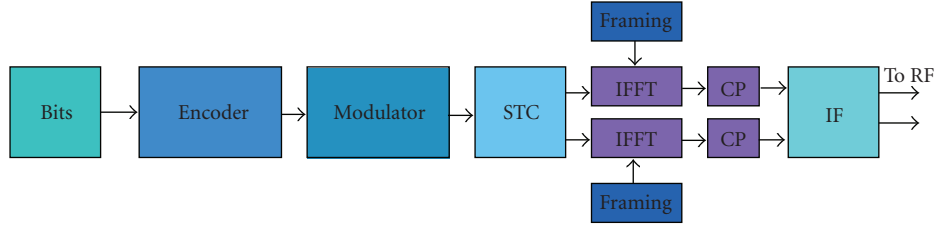
FIGURE 4: Base-Band and IF Transmitter Block diagram.
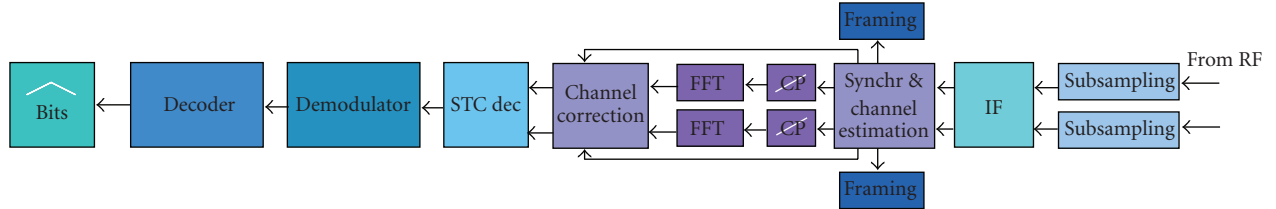
FIGURE 5: Base-Band and IF Receiver Block diagram.

testbed, a sampling frequency $f'_s = 50$ MHz was used. Since the signal bandwidth is 3.5 MHz, we can recover it without distortion.

In Figures 4 and 5, the complete block diagrams for the transmitter and receiver, respectively, are shown.

2.3.1. Transmitter. At the transmitter, first we obtain the bit sequence, which can be a specific one or generated randomly. Next, this bit sequence is passed through the encoder block which includes a randomizer, a Reed-Solomon (RS) encoder, an interleaver, and a puncturer to obtain the encoded bits. This block may change depending on the transmission mode. Besides, since there is an RS encoder, bits must be converted into bytes and, after the RS, converted back into bits, an operation that consumes registers in the FPGA. Also in this block, due to the interleaver, a SIRO (Sequential Input Random Output) buffer is needed.

After the encoder block, bits are fed to the modulator which generates the base-band I-Q complex signal. The modulation (BPSK, QPSK, 16QAM, or 64QAM) used again depends on the transmission mode.

Once the complex I-Q signal has been generated, in order to obtain spatial diversity, an Alamouti Space Time Coding (STC) scheme is applied; thus, two different streams are created, each one for each antenna. The framing structure such as preambles, pilots, and headers is appended to these two different flows and they are transformed into time-domain by using an IFFT. In order to avoid ICI (Inter-Carrier Interference) and ISI, the CP is added and we obtain the complex base-band signal. Subsequently, each branch is up-converted at 70 MHz intermediate frequency. It should be noted that the prototype does not include a DUC (Digital Up-converter); so this operation must be performed by the FPGA. These up-converted signals will be the inputs for the RF module.

One of the bottlenecks in the system is the IFFT/FFT processing. The IFFT module works synchronously using 256-symbol-long windows, which fits with the size of the data frame used. It should be noted that the data frame is only ready for processing at the end of the window, because this is when the 256 symbols have been collected. Once the block acquires the first 256 symbols, they are processed and the result is copied to the output line before the second window time has elapsed. It takes two thirds of the window time to make the necessary calculations. Thus, there is only one third of a window time to put the result in the output line. As the IFFT does not change the bit size of the data, it forces the system to increase threefold the bit ratio output as can be seen in Figure 6(a). While the input consists of a continuous trail of frames, the output shows a regular discontinuity formed by blank spaces with an equivalent length of two thirds of a window-time, followed by a frame of 256 symbols occupying the remaining third of the window delayed one-window-time. For this reason, a framer reshaper is used to remove the blanks and return the bit ratio back to that of the IFFT input. The data operation is also used to introduce the cyclic prefix (not showed in the figure). The reshaping described above introduces a one-window-time delay.

2.3.2. Receiver. On the receiver side, the cyclic prefix is extracted before the FFT module. The FFT module works the same way as its IFFT counterpart. However, there is an additional problem. To obtain symmetry between transmission and reception, the output of the FFT should be the same frames as at the input of the IFFT. If they are not, they cannot be delivered to the next module in the reception chain. Nevertheless, it can be observed that the output of the IFFT is also formed by the burst showed in the IFFT, with the additional inconvenience of the first symbol of the frame moved to the last position of the burst. The problem is solved using a frame reshaper similar to the one used on the transmitter side, with the additional feature of frame

(a) IFFT module

(b) FFT module
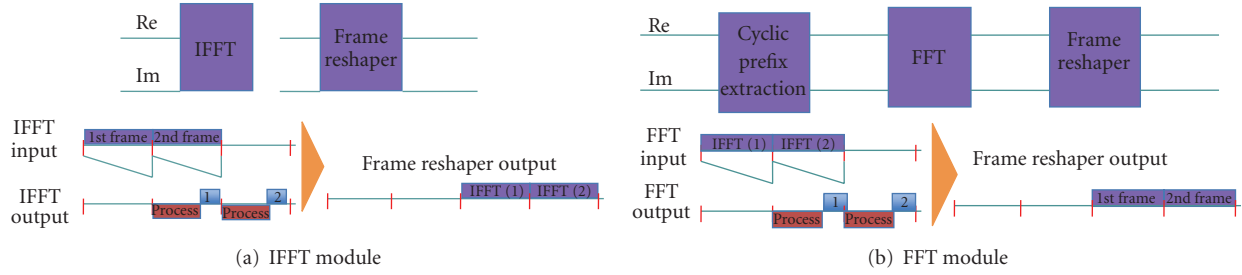
Figure 6: IFFT/FFT Reshaping module.

(a) Received Constellation

(b) Corrected Constellation
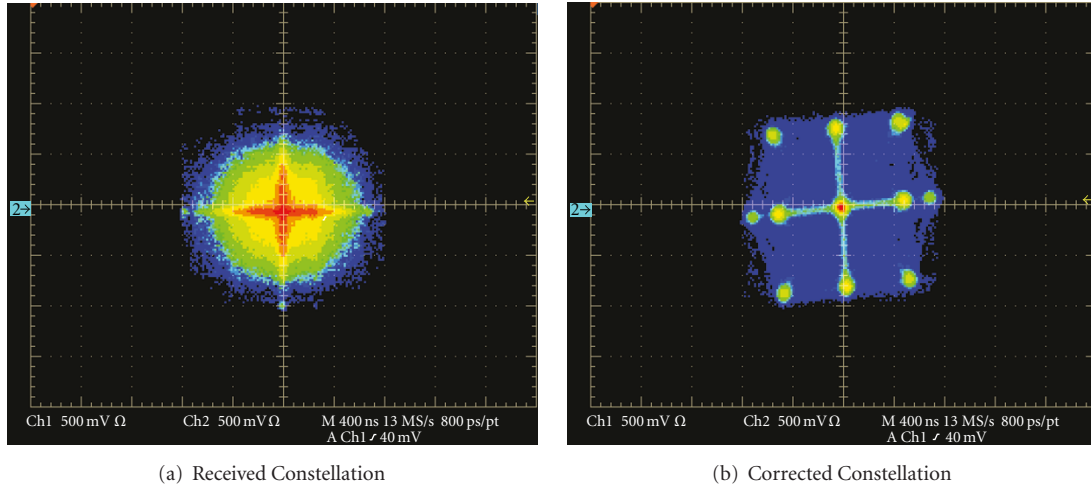
Figure 7: Constellations for QPSK at Antenna 1 at SNR = 20 dB.

inversion (see Figure 6(b)). It also introduces a one-window-time delay.

Moreover, during the testing period, a symbol error was usually detected in the final output, always affecting the first or the last symbol in a frame. As the first and the last symbols belong to the safe-guard space (due to the cyclic prefix), this error was never propagated to the following modules.

Besides, also on the receiver side, the counterparts blocks to those in the transmitter have been implemented but some extra blocks are also needed for synchronization (time and frequency) and channel estimation/equalization purposes. As mentioned before, since the ADC sample frequency does not fulfill the Nyquist criterion (the input signal is 70 MHz), a subsampling processing is performed previous to the IF block. Next, the signal is down-converted to baseband and introduced to the synchronization and channel estimation block. In this block, a joint time-frequency offset and channel estimation has been implemented based on [24], and also including the enhanced version.

Before frequency offset and channel estimation, a timing acquisition process is needed. The time synchronization has been implemented with a buffer and shift registers to perform the correlation metric. Based on triggered thresholds using algorithm [22], the block detects the beginning of the frame. Joint frequency offset and channel estimation algorithm is then executed as explained in Section 2.1. After

the frequency offset estimation procedure, its estimation is corrected by using the CORDIC (COordinate Rotation DIgital Computer) algorithm [26]. In this block, the framing information is also extracted. After this point, blocks in the receiver are the counterpart of those at the transmitter, including an efficient ad hoc Viterbi implementation for the decoder block.

In Figure 7(a) the received constellation at antenna 1 is shown, where a normalized frequency offset of $\varepsilon = 0.3$ has been induced. Next, in Figure 7(b), the corrected constellation by the frequency offset block at antenna 1 is also displayed. It can be seen that even though the normalized frequency offset is large, the algorithm is able to compensate it and it presents a good performance; the decision regions are well defined. In this figure, for a QPSK transmission, the pilot symbols (BPSK modulated at the edges) and the two superimposed QPSK constellations due to the Alamouti codification can be observed.

2.3.3. Implementation.

The prototyping has been carried out by using System Generator and ISE (Integrated System Environment) Foundations from Xilinx [27] starting with a Simulink design. After this first prototype, some parts such as the Viterbi decoder have been implemented directly in VHDL (Very high-speed integrated circuit Hardware

TABLE 2: Required FPGA resources summary.

Element	Slice	% Slice
Flip/Flops	4007	8
4 Input LUTs	5870	11
Logic Utilization Slice	4214	17
FIFO memories	0	0
RAM memories	2	1

Description Language) in order to speed up the design, reduce area, and improve performance.

In the following, to evaluate the buffer size, the whole transmission chain is described, taking as an example the transmission of a frame consisting of 10 OFDM symbols by using the transmission mode 1: BPSK at R_c = 1/2 code rate. Therefore, each OFDM symbol is made up of 96 bits. The total number of bits provided by the OFDM frame is 960. The Randomizer and the interleaving blocks do not affect the number of bits, because they are only data movements. The convolutional encoder block generates two data lines, with 960 bits per OFDM frame each. The puncturing block aggregates both lines, providing a single line conveying 1920 bits per OFDM frame. The BPSK modulation block generates a pair of I/Q lines (i.e., two lines) carrying 3840 bits per OFDM frame each.

Next, the STC block performs an Alamouti encoder operation in order to feed the two antennas, that is, the testbed doubles the data rate. The output of this block consists of two pair of I/Q lines (i.e., four lines), while the total number of bits implied per line remains the same. Afterwards, the pilots and safeguard insertion block introduce 64 additional subcarriers to be used as pilots and safeguard band. Each sub-carrier is made up of two bits. The result is an OFDM frame made up of 10 OFDM symbols of 256 two-bit sub-carriers each. This totals 5120 bits per OFDM frame allocated by each of the four lines.

The preamble insertion block adds the short preamble at the beginning of each frame to obtain the final OFDM frame. At this point, 5632 bits per OFDM frame are being transmitted by each line.

The IFFT block forces a fivefold bit expansion in order to allocate 8 decimal positions. Each two-bit sub-carrier is converted to a ten-bit (eight of which are decimals) subcarrier, totalling 28160 bits per OFDM frame in each of the four lines (i.e., 11 OFDM symbols, 256 sub-carriers per OFDM symbol, 10 bits per subcarrier).

The final cyclic prefix insertion block takes the last 320 bits of the 2560-bit symbol and copies them at the beginning of the symbol. As a result, each of the four lines transports 31680 bits per OFDM-transmitted frame.

A summary of the FPGA resources used by the prototype is shown in Table 2. From this table it can be seen that the implemented prototype only uses about 40% of the total platform, and therefore more than half of the space can be dedicated to implementing other functionalities or signal processing algorithms. Besides, most of the parts in the design are able to work above 100 MHz, except the IFFT/FFT block, which has the maximum frequency at 28 MHz. The reason is because the arranging of buffers (due to the mixture of preambles, data and pilots) to adapt data to the FFT block is difficult, as explained in Section 2.1. Since this block works at baseband and the bandwidth is 3.5 MHz, this frequency is more than enough.

3. Scenarios and Measurement System

3.1. Scenario. In order to perform the characterization and modeling of MIMO BFWA (Broadband Fixed Wireless Access) channels in outdoor-indoor environments, several measurement campaigns were carried out on the 3.5 GHz frequency band with a bandwidth of 250 MHz. The measurements were made between two buildings of the University of Cantabria (Spain) separated by a distance of 120 m. The transmitter array was positioned as a base station on the terrace of a building, while the receiver was placed inside the other building in three scenarios with different characteristics. The first scenario is an assembly room, an open area with few obstacles around the receiver array (denoted as open). The second scenario is an electronics laboratory equipped with computers, workbenches, measuring equipment, and cupboards (denoted as closed). These two scenarios are at a height around 6 m lower than the transmitter. The third scenario is a typical office floor, at a height of 15 meters below the transmitter. The influence of the line of sight between the transmitter and the receiver is considered in the channel characterization, placing the receiver array in three different local areas for each measurement scenario. The first measurement area was located close to a window, opposite the transmitter, in a QLOS (quasiline of sight) situation. In this area, the line of sight was only obstructed by a window. On moving away from this window and going into the room, the visual line of sight between the transmitter and the receiver was lost. In these conditions of nonline of sight, measurements are made in two local areas, NLOS (Nonline of Sight), in which the receiver is already indoors in the building but only one of the inner walls obstructs the direct sight of the transmitter, and HNLOS (Hard-NLOS), in which the transmitter is located in an indoor zone of the building with several partitions between the transmitter and the receiver.

3.2. Measurement System. A wideband measurements system based on an E4433B signal generator and an Agilent PNA E8362A network analyzer was used. The system performs a 400-tone frequency sweep in the band of interest: 3.385– 3.635 GHz. The two ends of the measurement system were synchronized in frequency and phase thanks to the external reference of 10 MHz generated by rubidium oscillators and disciplined by GPS (Global Positioning System) receivers.

The transmitter array was formed by directional sectorial antennas with a gain of 15 dBi separated 10λ and pointing towards the measurement scenario. The elements of the receiver array were two omnidirectional biconical antennas separated by 1.0λ with a typical gain of 0 dBi. The measurements were made in the absence of moving persons to maintain the stationarity of the channel.

(a) Laboratory

(b) Assembly Room + Office
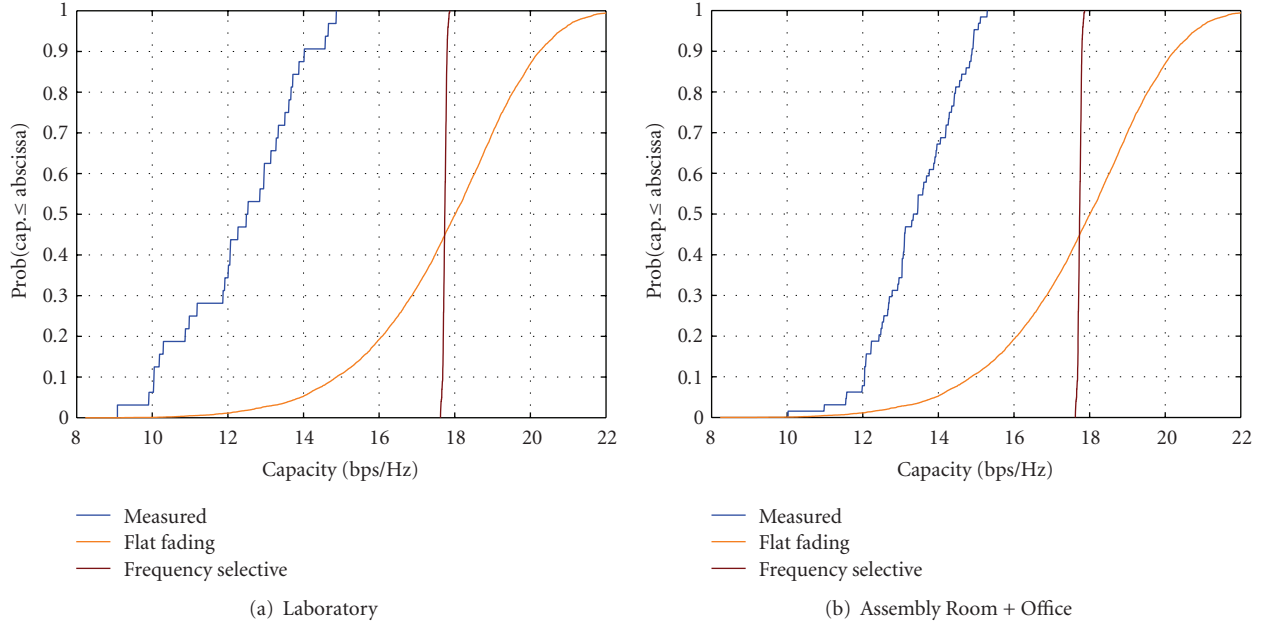
FIGURE 8: CDF of the MIMO channel capacity with SNR = 30 dB measured and modeled in LOS areas.

(a) Open Scenario

(b) Closed Scenario
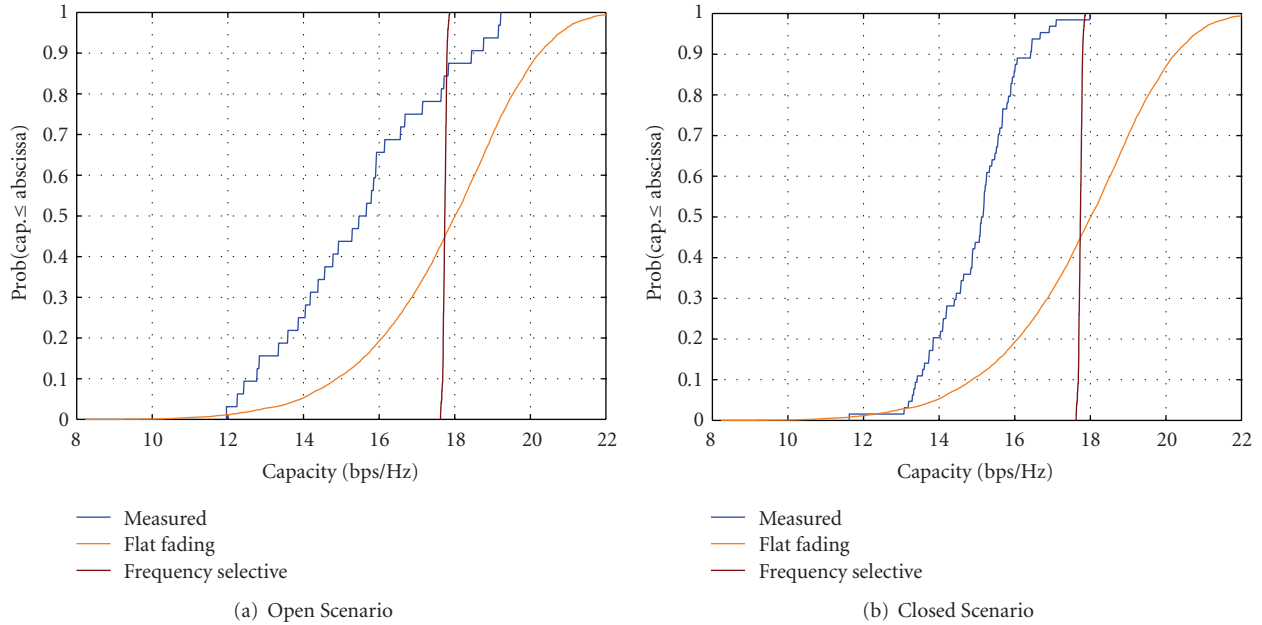
FIGURE 9: The MIMO channel capacity with SNR = 30 dB measured and modeled in NLOS areas.

3.3. Capacity in Measured 2×2 *MIMO Channels.* Figures 8, 9, and 10 show the results of measured capacity with perfect channel knowledge at the transmitter in the three scenarios previously described [28]. They also include the CDF (Cumulative Density Function) of the capacity obtained from two canonical wideband channel models used as a reference. These two canonical cases present uncorrelated Rayleigh fading in the spatial domain and two different degrees of correlation in the frequency domain, one totally flat in frequency (flat fading) and another totally selective

in frequency (frequency selective). The measured channels undergo the effect of the spatial and frequency correlation jointly and inseparably, always showing a lower capacity than that of the reference channels. It is worth noting that, for a constant SNR (Signal-to-Noise Ratio), when the situation goes from LOS to NLOS and then to the more obstructed HNLOS, the capacity curves are closer to the theoretical ones. This is due to the combination of two phenomena: the more obstructed situations, with higher levels of scattering, present less spatial correlation, and the greater temporal scattering

(a) Open Scenario

(b) Closed Scenario
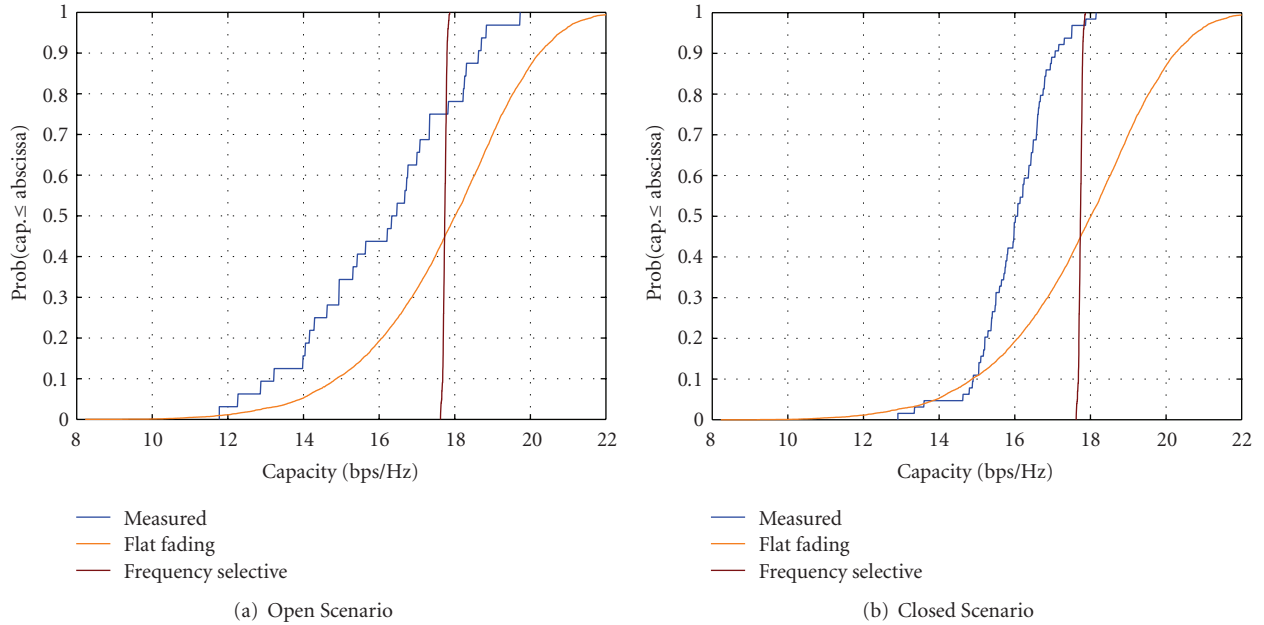
FIGURE 10: The MIMO channel capacity with SNR = 30 dB measured and modeled in HNLOS areas.

(a) Closed HNLOS scenario

(b) Closed LOS Scenario
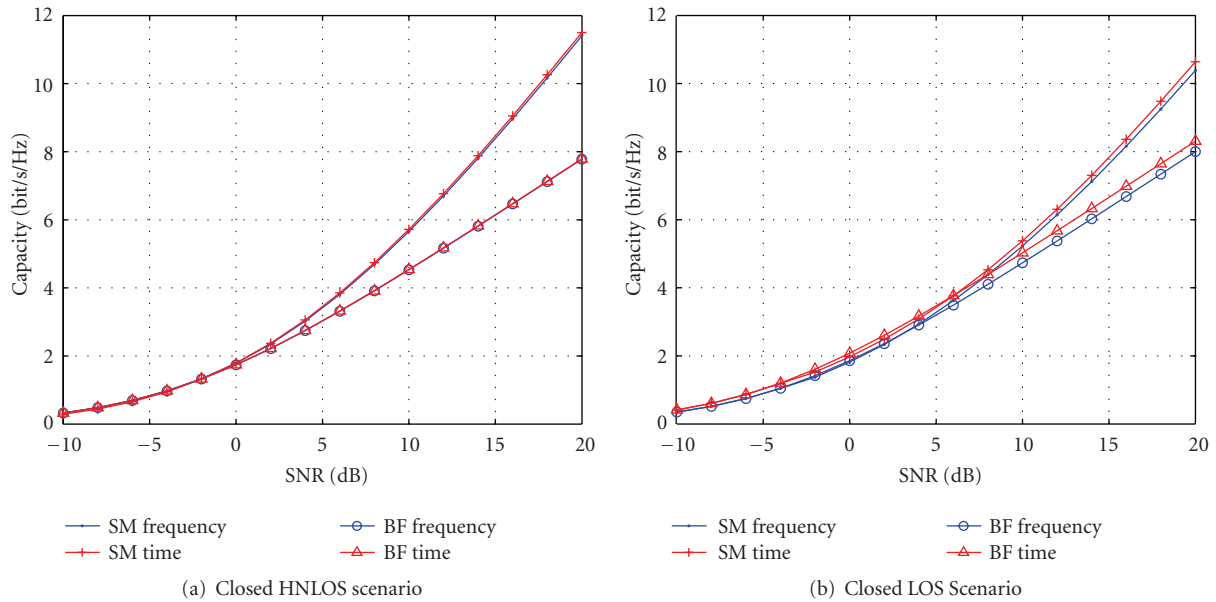
FIGURE 11: Average Capacity with frequency averaging versus time averaging.

means a greater diversity of frequency. The comparison of the capacity curves shows significant differences between measured and the canonical (theoretical) cases which do not consider the spatial correlation.

4. Capacity and BER Performance

In [29], we analyzed the average capacity that may be achieved in the measured channels and three transmission strategies: (i) exact channel knowledge, CSIT (Channel State Information at the Transmitter), (ii) knowledge about the channel statistics, CDIT (Channel Distribution Information at the Transmitter), and, in order to have a baseline for the comparisons, (iii) no channel knowledge. We concluded that the performance achieved in case of CDIT knowledge is very similar to the optimum when the transmitter knows the channel perfectly.

In MIMO-OFDM, the knowledge about the channel statistics may be obtained from either time or frequency averages. Calculating the average of the channel correlation in the time domain requires a certain amount of time intervals to be awaited in order to have a good estimation
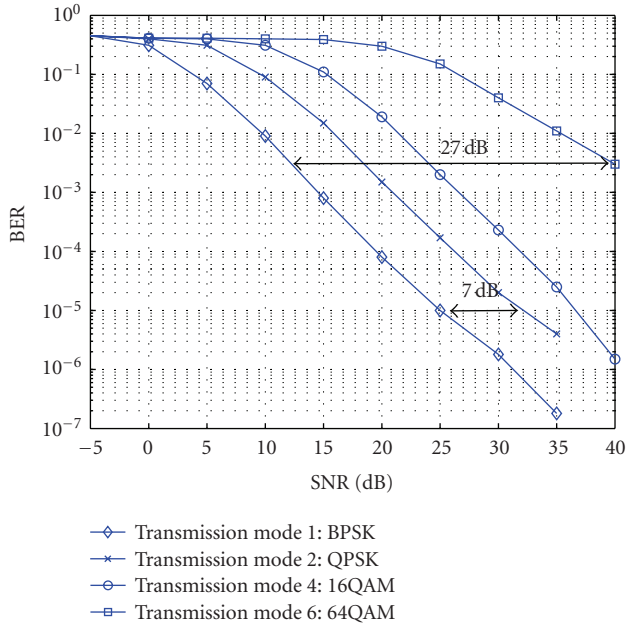
FIGURE 12: BER comparison for different IEEE 802.16 transmission modes using 2×2 MIMO.

(a) BER

(b) MSE

FIGURE 13: BER and MSE for transmission mode 1: BPSK. The label "Only Ch. Est." denotes the case when only channel estimation and compensation are used whereas "Enhanced Est." accounts for the joint enhanced channel and frequency offset estimation case.

of the true average. Therefore, we propose employing the frequency dimension offered by OFDM so that the average can be calculated in frequency with no temporal delay. Instead of using several time intervals to calculate the average, we perform the averaging through all the frequency samples that are available in a given OFDM symbol.

Figures 11(a) and 11(b) show the comparison of the two approaches when beamforming or spatial multiplexing is used. In this case 2000 time samples are used to calculate the average value of the correlation matrix on each subcarrier. On the other hand, 256 values obtained from the subcarriers of an OFDM symbol are used, and the calculated value is used through all the subsequent symbols, assuming that conditions in the channel are quasistatic. It can be seen that similar performance results have been obtained in both cases, even though when averaging in the frequency domain the considered number of different realizations is considerably smaller. Therefore, we can conclude that frequency averaging, which may eventually reduce the delay necessary to compute the channel statistics, is a good choice.

Comparing the average capacity in the HNLOS and LOS scenarios the same conclusions as in the previous section are obtained with higher capacity values realizable in HNLOS due to the lower spatial correlation. Interestingly, in this case, attaining the full capacity requires the use of all transmission degrees of freedom so that beamforming along the principal eigenvector gives substantially lower average capacity than spatial multiplexing at high SNR.

In Figure 12 the obtained BER (Bit Error Rate) under ideal channel estimation and perfect time and frequency synchronization for four out of 7 transmission modes is shown over an SUI-3 channel [30]. It can be seen that using BPSK, a BER about 10^{-5} is reached at SNR of 25 dB per
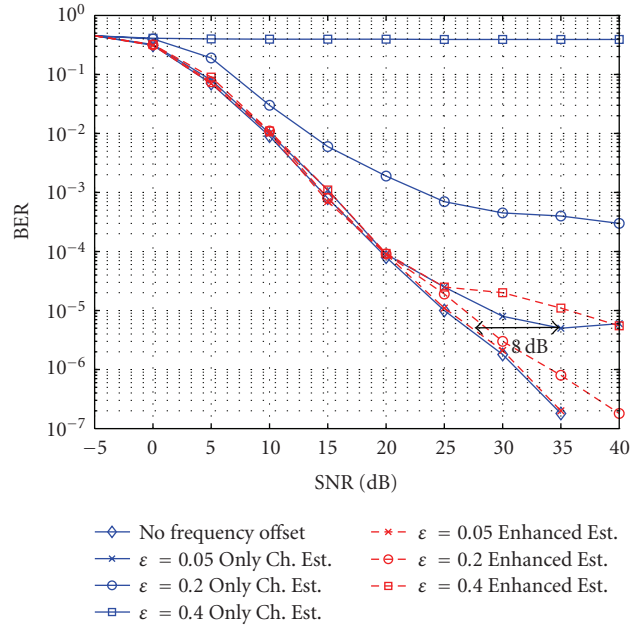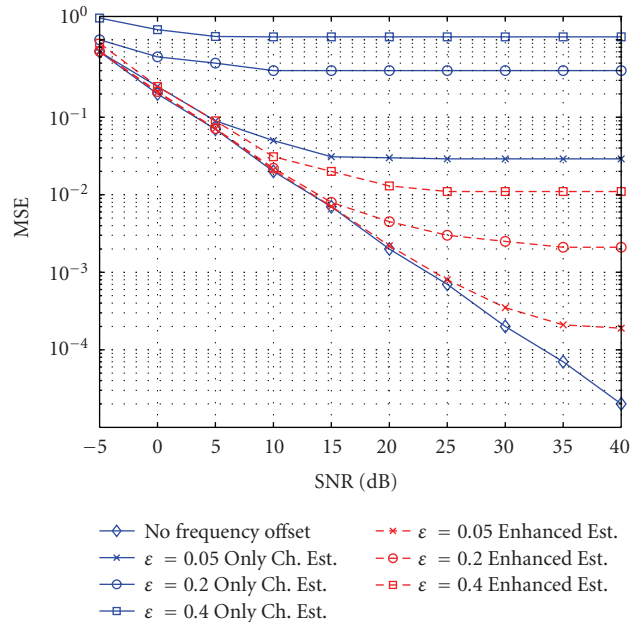
antenna. Besides, it can be observed that transmission mode 6 requires too much power and it will be ruled out of wireless NLOS or HNLOS outdoor-indoor transmission scenarios. It should be noted that here the data rate is double since each antenna transmits different pieces of information.

The BER and MSE for channel estimation are drawn in Figures 13(a) and 13(b), respectively. In those figures, the

performance, activating the joint frequency offset estimation/correction (enhanced), is shown. Two main conclusions can be extracted from these results. The first one is that without the frequency offset estimation, the system offers very poor results; a normalized frequency offset larger than 0.2 significantly degrades the performance (including error floor) and makes the system unusable. However, once the joint channel and frequency offset estimation algorithm is switched on, the performance remains as in a residual frequency offset of 0.05 (see Figure 13(a)). The second one is that although the MSE is large even when joint estimation is activated (see Figure 13(b)), performance is not seriously compromised.

5. Conclusions

In this paper, a real-time flexible 2×2 MIMO-OFDM IEEE 802.16 prototype that was implemented and a measurement campaign on the 3.5 GHz band have been described. For the baseband, an FPGA architecture was used, showing that this hardware is adequate for prototyping wide-band wireless communications systems. It has been shown that since we used the same pipeline for the transmitted/received data (out of the STC), the FPGA is efficiently utilized at the expenses of larger buffers (data vectors are processed concatenated).

The analysis of measured channels showed that higher capacity can be achieved in case of obstructed scenarios and that CDIT capacity is close to CSIT with much lower complexity and requirements in terms of channel estimation and feedback. The channel correlation can be obtained from averages in the frequency domain that may eventually reduce the delay necessary to compute the channel statistics. Finally we have shown that for MIMO-OFDM systems, extra signal processing such as enhanced joint channel and frequency offset estimation is needed to obtain a good performance and approach in practice the theoretical capacity improvements. In the future, the evaluation of different transmission schemes and diversity configurations will be carried out by using the prototype.

Acknowledgments

References

[1] S. Nanda, R. Walton, J. Ketchum, M. Wallace, and S. Howard, "A high-performance MIMO OFDM wireless LAN," *IEEE Communications Magazine*, vol. 43, no. 2, pp. 101–109, 2005.

[2] T. J. Willink, "MIMO OFDM for broadband fixed wireless access," *IEE Proceedings: Communications*, vol. 152, no. 1, pp. 75–81, 2005.

[3] IEEE 802.16 Working Group on Broadband Wireless Access Standards (WirelessMAN), http://www.http.com//ieee802.org/16.

[4] IEEE 802.16-2004, "IEEE standard for local and metropolitan area networks Part 16: air interface for fixed broadband wireless access systems," Tech. Rep., IEEE, 2004.

[5] IEEE 802.16e-2005, "IEEE standard for local and metropolitan area networks Part 16: air interface for fixed and mobile broadband wireless access systems. Amendment 2: physical and medium access control layers for combined fixed and mobile operation in licensed bands and corrigendum 1," Tech. Rep., IEEE, 2005.

[6] P. Murphy, F. Lou, A. Sabharwal, and J. P. Frantz, "An FPGA based rapid prototyping platform for MIMO systems," in *Proceedings of the 37th Asilomar Conference on Signals, Systems and Computers (ACSSC '03)*, pp. 900–904, Pacific Grove, Calif, USA, November 2003.

[7] J. W. Wallace, B. D. Jeffs, and M. A. Jensen, "A real-time multiple antenna element testbed for MIMO algorithm development and assessment," in *Proceedings of IEEE International Symposium on Antennas and Propagation Society (APS '04)*, vol. 2, pp. 1716–1719, Monterey, Calif, USA, June 2004.

[8] M. Rupp, C. Mehlführer, S. Caban, R. Langwieser, L. W. Mayer, and A. L. Scholtz, "Testbeds and rapid prototyping in wireless system design," *EURASIP Newsletter*, vol. 17, no. 3, pp. 32–50, 2006.

[9] S. Caban, C. Mehlführer, R. Langwieser, A. L. Scholtz, and M. Rupp, "Vienna MIMO testbed," *EURASIP Journal on Applied Signal Processing*, vol. 2006, Article ID 54868, 13 pages, 2006.

[10] G. D. Golden, C. J. Foschini, R. A. Valenzuela, and P. W. Wolniansky, "Detection algorithm and initial laboratory results using V-BLAST space-time communication architecture," *Electronics Letters*, vol. 35, no. 1, pp. 14–16, 1999.

[11] R. M. Rao, W. Zhu, S. Lang, et al., "Multi-antenna testbeds for research and education in wireless communications," *IEEE Communications Magazine*, vol. 42, no. 12, pp. 72–81, 2004.

[12] H. Sampath, S. Talwar, J. Tellado, V. Erceg, and A. Paulraj, "A fourth-generation MIMO-OFDM broadband wireless system: design, performance, and field trial results," *IEEE Communications Magazine*, vol. 40, no. 9, pp. 143–149, 2002.

[13] C. Dubuc, D. Starks, T. Creasy, and Y. Hou, "A MIMO-OFDM prototype for next-generation wireless WANs," *IEEE Communications Magazine*, vol. 42, no. 12, pp. 82–87, 2004.

[14] W. Xiang, T. Pratt, and X. Wang, "A software radio testbed for two-transmitter two-receiver space-time coding OFDM wireless LAN," *IEEE Communications Magazine*, vol. 42, no. 6, pp. S20–S28, 2004.

[15] W. Xiang, D. Waters, T. G. Pratt, J. Barry, and B. Walkenhorst, "Implementation and experimental results of a three-transmitter three-receiver OFDM/BLAST testbed," *IEEE Communications Magazine*, vol. 42, no. 12, pp. 88–95, 2004.

[16] S. Haene, D. Perels, and A. Burg, "A real-time 4-stream MIMO-OFDM transceiver: system design, FPGA implementation, and characterization," *IEEE Journal on Selected Areas in Communications*, vol. 26, no. 6, pp. 877–889, 2008.

[17] IEEE 802.11a, "WLAN medium access control (MAC) and physical layer (PHY) specifications: high-speed physical layer in the 5 GHz Band," Tech. Rep., IEEE, June 2001.

[18] S. M. Alamouti, "A simple transmit diversity technique for wireless communications," *IEEE Journal on Selected Areas in Communications*, vol. 16, no. 8, pp. 1451–1458, 1998.

[19] V. Tarokh, H. Jafarkhani, and A. R. Calderbank, "Space-time block codes from orthogonal designs," *IEEE Transactions on Information Theory*, vol. 45, no. 5, pp. 1456–1467, 1999.

[20] V. P. G. Jiménez, M. J. F.-G. García, F. J. González Serrano, and A. García Armada, "Design and implementation of synchronization and AGC for OFDM-based WLAN receivers,"

IEEE Transactions on Consumer Electronics, vol. 50, no. 4, pp. 1016–1025, 2004.

[21] T. M. Schmidl and D. C. Cox, "Robust frequency and timing synchronization for OFDM," *IEEE Transactions on Communications*, vol. 45, no. 12, pp. 1613–1621, 1997.

[22] H. Minn, V. K. Bhargava, and K. B. Letaief, "A robust timing and frequency synchronization for OFDM systems," *IEEE Transactions on Wireless Communications*, vol. 2, no. 4, pp. 822–839, 2003.

[23] T.-L. Tung and K. Yao, "Channel estimation and optimal power allocation for a multiple-antenna OFDM system," *EURASIP Journal on Advances in Signal Processing*, vol. 2002, no. 3, pp. 330–339, 2002.

[24] N. Balamurali and D. Jalihal, "An efficient algorithm for joint carrier frequency offset and channel estimation in IEEE 802.16 OFDM systems," in *Proceedings of the 1st International Symposium on Wireless Communication Systems (ISWCS '04)*, pp. 428–432, Port Louis, Mauritius, September 2004.

[25] W. H. Nicholson and A. A. Sakla, "The sampling and full reconstruction of band-limited signals at sub-Nyquist rates," in *Proceedings of the IEEE International Symposium on Circuits and Systems (ISCS '90)*, vol. 3, pp. 1796–1800, New Orleans, La, USA, May 1990.

[26] R. Andraka, "A survey of CORDIC algorithms for FPGA based computers," in *Proceedings of the ACM/SIGDA International Symposium on Field Programmable Gate Arrays (FPGA '98)*, pp. 191–200, Monterey, Calif, USA, February 1998.

[27] Xilinx, "ISE Foundations," http://www.xilinx.com/tools/designtools.htm.

[28] O. Fernández, M. Domingo, and R. P. Torres, "Outdoor to indoor 2×2 wideband MIMO channel modelling," in *Proceedings of the IEEE 69th Vehicular Technology Conference (VTC '09)*, pp. 1–5, Barcelona, Spain, April 2009.

[29] J. J. G. Fernández, M. Sánchez-Fernández, A. G. Armada, R. P. Torres, M. Domingo, and O. Fernández, "Analysis of beamforming and spatial multiplexing strategies in WMAN outdoor-indoor scenarios," in *Proceedings of the IEEE 69th Vehicular Technology Conference (VTC '09)*, pp. 1–5, Barcelona, Spain, April 2009.

[30] K.V. S. Hari, K. P. Sheikh, and C. Bushue, "Interim channel models for G2 MMDS fixed wireless applications," Tech. Rep. 802.16.3c-00/49r2, IEEE, 2000.